Optics Letters

Chirp-controlled filamentation and formation of light bullets in the mid-IR

V. Shumakova,[1] S. Ališauskas,[1] P. Malevich,[1] A. A. Voronin,[2,3] A. V. Mitrofanov,[2,3,4] D. A. Sidorov-Biryukov,[2,3,4] A. M. Zheltikov,[2,3,4,5] D. Kartashov,[6] A. Baltuška,[1,7] and A. Pugžlys[1,7,*]

[1]Photonics Institute, TU Wien, Gusshausstrasse 27-387, A-1040 Vienna, Austria
[2]Physics Department, International Laser Center, M. V. Lomonosov Moscow State University, Moscow 119992, Russia
[3]Russian Quantum Center, ul. Novaya 100, Skolkovo, Moscow Region 143025, Russia
[4]Kurchatov Institute National Research Center, Moscow 123182, Russia
[5]Department of Physics and Astronomy, Texas A&M University, College Station, Texas 77843-4242, USA
[6]Friedrich-Schiller University Jena, Max-Wien Platz 1, 07743 Jena, Germany
[7]Center for Physical Sciences & Technology, Savanoriu Ave. 231, LT-02300 Vilnius, Lithuania
*Corresponding author: pugzlys@tuwien.ac.at

Received 11 February 2019; revised 20 March 2019; accepted 26 March 2019; posted 29 March 2019 (Doc. ID 359859); published 18 April 2019

Formation of light bullets—tightly localized in space and time light packets, retaining their spatiotemporal shape during propagation—is, for the first time, experimentally observed and investigated in a new regime of mid-infrared filamentation in ambient air. It is suggested that the light bullets generated in ambient air by multi-mJ, positively chirped 3.9-μm pulses originate from a dynamic interplay between the anomalous dispersion in the vicinity of CO_2 resonance and positive chirp, both intrinsic, carried by the driver pulse, and accumulated, originating from nonlinear propagation in air. By adjusting the initial chirp of the driving pulses, one can control the spatial beam profile, energy losses, and spectral-temporal dynamics of filamenting pulses and deliver sub-3-cycle mid-IR pulses in high-quality beam on a remote target.

https://doi.org/10.1364/OL.44.002173

Many nonlinear spectroscopic techniques, such as remote laser induced breakdown spectroscopy (LIBS) [1], nonlinear light-imaging, detection and ranging (LIDAR), multidimensional spectroscopy in molecular fingerprint region, and others require targeted delivery of intense light with suitable pulse duration and energy, as well as of good beam quality. Often this task is complicated by atmospheric turbulences, causing random variations of the refractive index and resulting in fluctuations of light intensity on the target [2,3]. Propagation of light in filamentation regime, when light intensity is clamped, to a certain extent helps to overcome this problem but brings new challenges linked to plasma formation, followed by an energy loss and a temporal pulse splitting [4]. Another limitation of filamentation-based beam delivery is an onset of multiple filamentation, caused by modulation instabilities, which have a random character and result in small-scale beam distortions. Multiple filamentation occurs when pulse peak power P_{peak} is much higher than the critical power of self-focusing P_{cr} ($P_{peak} \gtrsim 10P_{cr}$ [5]). Because of that, in the case of 40-fs 800-nm pulses the energy contained in a single filament in ambient air is limited at a sub-mJ level [6]. Temporal pre-chirping of the driver pulses helps to achieve filamentation at a remote position in space [7] and increases the maximum energy, which is possible to transport in a single filamentation regime up to 1–2 mJ [8] but does not eliminate plasma-related problems.

The situation changes substantially when the wavelength of the driving pulses increases. Since P_{cr} scales as a square of the wavelength, considerably more energy can be deposited in a single filament driven by mid-IR pulses. Furthermore, mid-IR spectral range is beneficial because of the lower ionization rates and higher resistance for the modulation instabilities [9]. Due to the larger diameter [9,10], mid-IR filaments are less sensitive to random refractive index fluctuations and small natural atmospheric obstacles, such as water droplets. Finally, a unique combination of high atmospheric transparency and anomalous dispersion of air in certain mid-IR spectral windows promotes an opportunity for a lossless delivery of high-energy pulse [11] and simultaneous solitonic self-compression [12,13], which leads to boosted intensity at the position of a remote target, important for the generation of coherent supercontinuum [14,15], intense THz radiation [16], and of higher order harmonics [17]. On the other hand, multiple molecular resonances characteristic for the mid-IR "fingerprint" spectral region not only determine anomalous dispersion windows but also complicate propagation because of absorption losses, which can be dramatically enhanced via nonlinear spectral broadening [15,18].

One of the atmospheric transparency windows is situated between the resonances at 3.2 μm and 4.2 μm [19,20], corresponding to the absorption of water vapor (H_2O) and carbon dioxide (CO_2), respectively, which makes feasible lossless propagation of laser pulses with the central wavelength in this spectral range. Furthermore, because of anomalous dispersion of air between 3.6 and 4.2 μm [19,20], solitonic self-compression

of mid-IR pulses [13] and even, as it was predicted by numerical simulations [9,21], formation of light bullets (LBs)—highly localized in space and time light packets preserving their spatial and temporal characteristics during the propagation [22]—is possible.

Here we report on the first, to the best of our knowledge, experimental observation of the mid-IR LBs in ambient air. We show that through the self-compression in the filaments mid-IR pulses with a duration of 28–32 fs in a symmetric beam profile can be generated on the remote target with significant suppression of the nonlinearly enhanced absorption losses.

Experimental studies were performed by employing a setup presented in Fig. 1. Mid-IR pulses centered at 3.9 μm with energy of up to 30 mJ and duration of 80 fs were generated in an optical parametric chirped pulse amplification (OPCPA) system based on potassium titanyl arsenate (KTA) nonlinear crystals [18,23]. Filamentation was assisted by a loose focusing of the pulses with a spherical mirror with the focal length of $f = 7$ m. The implementation of a loose focusing allows to overcome the divergence of the beam and achieve filamentation without strong plasma formation on a laboratory scale [17,23]. The absence of strong plasma was confirmed by a homogeneity of spatial-spectral distribution, the absence of a donut-shape beam profile [24], which is typical in the case of strong plasma refraction, and by a rather weak signal of the plasma capacity probe [25]. In the case, when plasma cannot be observed visually, filamentation manifests itself by self-channeling occurring after energy exceeds 20 mJ. However, a self-symmetrization of initially elliptical beam starts already at the pulse energy of 10 mJ.

A chirp of the mid-IR pulses was varied by adjusting the grating compressor of the OPCPA system, which enables tuning of the pulse duration from ~80 fs to ~3 ps. Temporal pulse characterization was performed with second harmonic generation frequency resolved optical gating (SHG FROG) setup based on 200-μm-thick silver thiogallate (AGS) crystal. In order to avoid spatio-temporal distortions during propagation, the pulses at different positions along the filament were 4-f reimaged on the AGS crystal with spherical mirrors. The spectra were recorded with a scanning monochromator (Digikrom, CVI) and a liquid nitrogen cooled mercury cadmium telluride (MCT)-photodetector. Spatial beam profiles were detected with a pyroelectric camera (Spiricon Pyrocam III).

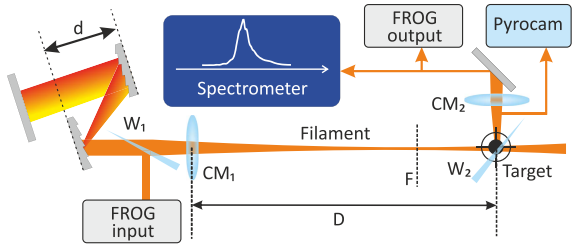

Fig. 1. Schematics of the experimental setup: FROG input/FROG output—SHG FROG setup for characterization of the pulses directly after compressor of OPCPA system and at the position of imaginary target, respectively; d, the distance between the gratings in the compressor; CM_1, curved mirror, assisting filamentation, $f = 7$ m; CM_2, reimaging curved mirror; $W_{1,2}$, attenuating CaF_2-wedges; D, the distance between CM_1 and the position of a "Target"; F, the position of the linear focus.

We have set the position of an imaginary target at the distance of ~8.5 m from the focusing mirror, which was limited by the length of our laboratory. The spectra, temporal pulse profiles as well as spatial beam profiles were recorded at different energies of optimally compressed 80 fs, 3.9 μm pulses. Already at the pulse energy of 11 mJ a red shift of the spectrum typical for stimulated rotational Raman scattering (SRRS) is observed [Figs. 2(a)–2(c)]. Because of the red shift, the spectrum starts to overlap effectively with the CO_2-absorption band, located in the vicinity of 4.2 μm, what leads to an enhancement of energy loss. Since the red-shifted pulses experience larger group velocity dispersion (GVD), they spread in time faster, and at the energy of 14 mJ pulse duration reaches 280 fs [Figs. 2(d)–2(f)]. With further increase of pulse energy, temporal splitting of the pulse takes place. Wigner distributions, calculated from the experimental SHG FROG traces, exhibit that the short-wavelength side of the pulse (3.5–3.9 μm) has a flat spectral phase due to a compensation of SPM-governed positive chirp by the weak anomalous dispersion of air. At the same time, long-wavelength components are stretched in time due to the steeper GVD near the CO_2 resonance. When the pulse energy exceeds 20 mJ [Figs. 2(g)–2(i)], pulses on the target split into 2 sub-pulses with the durations of 50 and 90 fs, which is preserved with further increase of input pulse energy. With further increase of energy, a separation between the two sub-pulses remains constant as relative depletion of the sub-pulse containing red spectral components takes place because of the Raman enhanced absorption losses (REAL) [18]. Therefore, without a control over the spectral broadening during propagation, only limited-energy pulses can be delivered on the remote target.

A propagation and spectral broadening of mid-IR pulses in the vicinity of molecular resonance makes filamentation extremely sensitive to the initial pulse duration and temporal chirp. Linearly chirped Gaussian pulse can be described as $E_p = \exp(-\frac{(1+iC)}{2}\frac{t^2}{\tau_0^2})$, where τ_0 is the transform-limited (TL) pulse duration and C is the chirp parameter. During a propagation in dispersive media pulse duration is changing $\tau_p = \tau_0\sqrt{(1+\frac{C\beta_2 z}{\tau_0^2})^2 + (\frac{\beta_2 z}{\tau_0^2})^2}$ with z being the propagation distance and β_2—the GVD [26]. An increase of the pulse duration, in accordance with the Margburger's equation [27], results in a smaller Kerr additive to the refractive index and hence to a later onset of filamentation. Furthermore, since air has

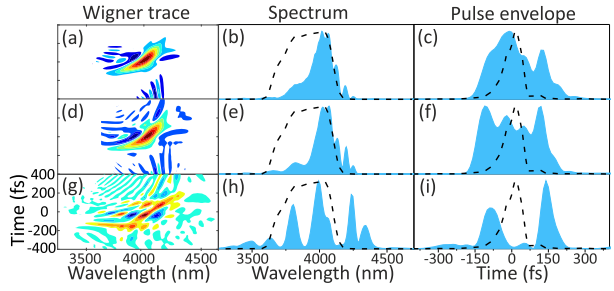

Fig. 2. Wigner distributions (a), (d), (g); spectra (b), (e), (h); and temporal pulse envelopes (c), (f), (i) of 11 mJ (a)–(c); 14 mJ (d)–(f); and 21 mJ (g)–(i) pulses after ~8.5 m of propagation in air in filamentation regime. Initial (at the output of the OPCPA system) pulse spectrum and envelope are shown by dashed black lines.

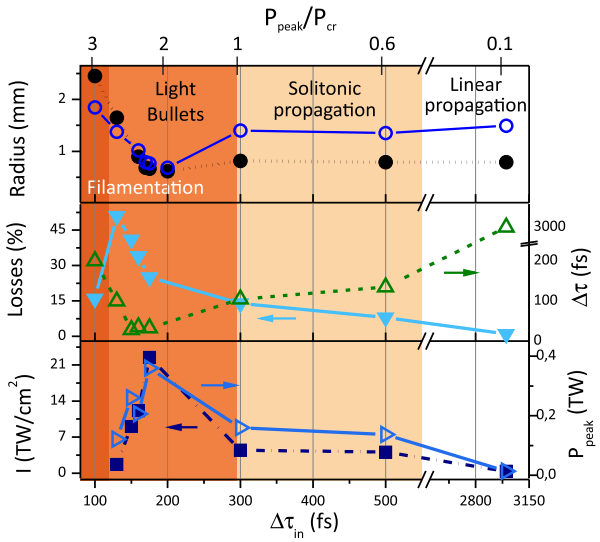

Fig. 3. Dependence of beam radii in the x- and y-directions, pulse duration, energy losses $(E_{in} - E_{out})/E_{in} \times 100\%$ (E_{in} is the pulse energy before the filament, E_{out} is the energy after the filament at 8.5 m distance from the focusing mirror), intensity, and peak power at "target" position on input pulse duration.

a negative GVD in the spectral region of 3.6–4.2 μm, a positive chirp of 3.9-μm pulses is compensated by the negative dispersion of air, which means that positively chirped pulses compress when propagating and reach their TL pulse duration at the propagation distance of $z_{min} = L_D|C|/(1 + C^2)$, $L_D = \tau^2/|\beta_2|$ is the dispersion length [24].

Initial pre-chirping of pulses also influences the SRRS-induced frequency downshift due to the reduction of overlap of spectral components in time. The frequency downshift plays a double role, as it is responsible for a dynamic increase of the dispersion and, hence, shortening of L_D and z_{min} [13] and, at the same time, for the buildup of the REAL (Fig. 3), which results in a loss of pulse energy.

Figure 3 illustrates a complicated interplay between the various nonlinear processes when the duration of positively chirped 29.5-mJ input pulse varies from 100 fs to 3 ps. In the case when the duration of the stretched pulse is in the range of 150–180 fs, at the distance of 8.5 m from the focusing mirror an efficient self-compression down to 28 fs can be achieved [Figs. 4(a)–4(c)]. In the case of 180-fs input pulse the energy losses decrease to ∼20%, which is more than two times lower compared to the losses when the pulse is stretched to 130 fs. Self-compressed pulses retain in the main peak 60%–70% of the pulse energy, which results into a high peak power reaching 340 GW and intensity of >20 TW/cm^2. This demonstrates a possibility to deliver high intensity mid-IR light on a remote target. Furthermore, if an initial beam has an asymmetric (elliptical) shape, it is self-symmetrized as a consequence of filamentation, resulting in a round spot with the diameter of ∼1 mm at a full width at half maximum (FWHM) level [Fig. 5(d)]. In the case when pulses are stretched less than to 150 fs, the beam on the target nucleates in the direction of the initial ellipticity [28]. When input pulses are stretched to more than 300 fs, the peak power drops below the critical value and filamentation does not occurs. This is evidenced by the beam profile, which at "the target" is elliptical as in the case of linear propagation [Fig. 4(h)]. Although for pulses with the durations ranging from ∼300 to ∼600 fs spatial localization is not achieved, a partial compensation of diffraction, which is due to the Kerr lens, and negative GVD of air enables quasi-1D solitonic nonlinear dynamics in the beam resulting in self-compression and strong temporal localization of the field [29]. Here we observe 3-fold self-compression of 3.9 μm mid-IR pulses from >300 fs down to ∼100 fs and significantly reduced nonlinear losses (from 50% to ∼10%) compared to the filamentation regime (Fig. 4). The losses and spectral changes completely vanish when the input pulses are stretched to a duration of a few picoseconds where the influence of SRRS becomes negligible [30].

Formation of the light bullets along the filament was observed in the case of positively chirped pulses with the duration of 130 fs (Fig. 5). At the distance of ∼3.5 m from the focusing mirror, pulse duration decreases to 90 fs, while the radius of the beam becomes smaller than 1 mm

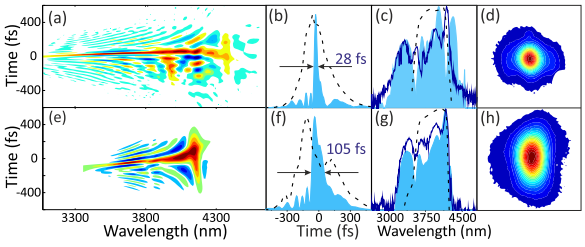

Fig. 4. (a) Wigner distributions (a), (e); temporal pulse profiles (b), (f); spectra (c), (g); and beam profiles (d), (h) of the pulse at a target position in case of filamentation (a)–(d) and formation of temporal 1D-solitons (e)–(h). Blue shaded areas in (b), (c), (f), and (g) correspond to the data retrieved from SHG FROG traces, as dark blue lines are the experimentally measured spectra. Black dashed lines are the pulse profiles and spectra measured before the filament.

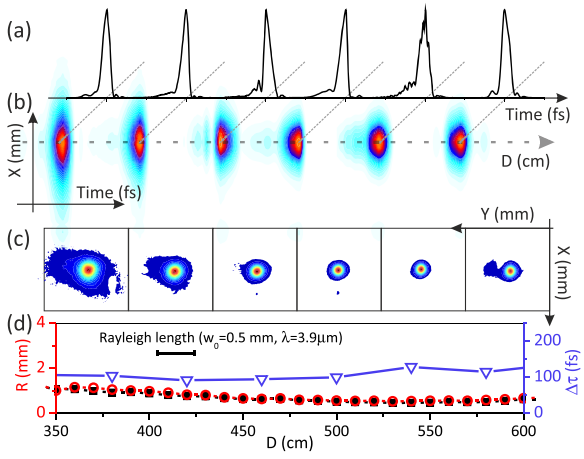

Fig. 5. Illustration of the formation of LBs. Evolution along the propagation of: temporal pulse profiles (a), longitudinal (Time) and transversal (X) intensity distribution (b), measured beam profiles (c), beam-radii at the level of $1/e^2$ in x-(open circles) and y- (solid squares) directions as well as of pulse duration (open triangles) (d); the Rayleigh length is calculated for the beam waist radius of 0.5 mm, corresponding to $1/e^2$ intensity level and determining the area containing of ∼80% of total energy.

[Fig. 5(d)]. Then, the temporal shape of the pulse and the beam profile remain similar over approximately 3 m of propagation [Figs. 5(a)–5(c)]. Note, that over the same distance, which is around 15 times larger than the Rayleigh length z_R for such beam waist ($z_R \sim 20$ cm in the case of $w_0 = 0.5$ mm), the pulse preserves its duration [Fig. 4(d)], which, in combination with the spatial localization, is a feature of LBs.

In conclusion, by adjusting the temporal chirp one can control energy, duration, spectrum, and spatial mode along propagation of 3.9-μm mid-IR pulses undergoing filamentation. A positive pre-chirping of 80-fs pulses to the duration of 150 fs leads to a self-compression down to 28 fs on a remote target, which is due to the interplay between spectral broadening originating from SPM and SRRS, dynamic spectral shift originating from SRRS, and the negative dispersion of air. As dispersion gets stronger with a red shift of the spectrum because of SRRS, the positive chirping leads to the postponed onset of filamentation and self-compressed pulses are delivered on a remote target in a symmetric round mode with a significant reduction of losses. The self-compression of chirped pulses in filaments with a negligible amount of plasma [18] leads to more homogeneous distribution of the spectral content across the beam. Finally, we present for the first time, to the best of our knowledge, experimental evidence of filament-assisted formation of mid-IR light bullets in air. The LBs are formed due to both a balance between the spectral-broadening and self-compression in negatively dispersed air, which leads to a soliton like dynamics of femtosecond mid-IR pulses in filaments and spatial beam self-trapping in the filament.

Funding. Austrian Science Fund (FWF) (P 26658, P 27577); Russian Foundation for Basic Research (RFBR) (16-02-00843, 17-52-53092, 18-29-20031, 19-02-00473); Welch Foundation (A-1801-20180324); Russian Science Foundation (RSF) (17-12-01533); Office of Naval Research (ONR) (00014-16-1-2578).

REFERENCES

1. T. A. Labutin, V. N. Lednev, A. A. Ilyin, and A. M. Popov, J. Anal. At. Spectrom. **31**, 90 (2016).
2. J. Peñano, J. P. Palastro, B. Hafizi, M. H. Helle, and G. P. DiComo, Phys. Rev. A **96**, 013829 (2017).
3. A. Houard, M. Franco, B. Prade, A. Durécu, L. Lombard, P. Bourdon, O. Vasseur, B. Fleury, C. Robert, V. Michau, A. Couairon, and A. Mysyrowicz, Phys. Rev. A **78**, 033804 (2008).
4. A. Mysyrowicz, A. Couairon, and U. Keller, New J. Phys. **10**, 025023 (2008).
5. A. Couairon and A. Mysyrowicz, Phys. Rep. **441**, 47 (2007).
6. W. Liu and S. Chin, Opt. Express **13**, 5750 (2005).
7. R. Nuter, S. Skupin, and L. Bergé, Opt. Lett. **30**, 917 (2000).
8. O. Varela, B. Alonso, I. J. Sola, J. S. Román, A. Zaïr, C. Méndez, and L. Roso, Opt. Lett. **35**, 3649 (2010).
9. P. Panagiotopoulos, P. Whalen, M. Kolesik, and J. V. Moloney, Nat. Photonics **9**, 543 (2015).
10. D. Mongin, V. Shumakova, S. Ališauskas, E. Schubert, A. Pugžlys, J. Kasparian, J. P. Wolf, and A. Baltuška, Appl. Phys. B **122**, 267 (2016).
11. P. Panagiotopoulos, M. Kolesik, and J. V. Moloney, Phys. Rev. A **94**, 033852 (2016).
12. B. Shim, S. E. Schrauth, and A. L. Gaeta, Opt. Express **19**, 9118 (2011).
13. A. A. Voronin and A. M. Zheltikov, Phys. Rev. A **95**, 023826 (2017).
14. D. Kartashov, S. Ališauskas, A. Pugžlys, A. Voronin, A. Zheltikov, M. Petrarca, P. Béjot, J. Kasparian, J.-P. Wolf, and A. Baltuška, Opt. Lett. **37**, 3456 (2012).
15. N. A. Panov, D. E. Shipilo, V. A. Andreeva, O. G. Kosareva, A. M. Saletsky, H. Xu, and P. Polynkin, Phys. Rev. A **94**, 041801 (2016).
16. V. Y. Fedorov and S. Tzortzakis, Opt. Express **26**, 31150 (2018).
17. A. V. Mitrofanov, A. A. Voronin, S. I. Mitryukovskiy, D. A. Sidorov-Biryukov, A. Pugžlys, G. Andriukaitis, T. Flöry, E. A. Stepanov, A. B. Fedotov, A. Baltuška, and A. M. Zheltikov, Opt. Lett. **40**, 2068 (2015).
18. V. Shumakova, S. Ališauskas, P. Malevich, C. Gollner, A. Baltuška, D. Kartashov, A. M. Zheltikov, A. V. Mitrofanov, A. A. Voronin, D. A. Sidorov-Biryukov, and A. Pugžlys, Opt. Lett. **43**, 2185 (2018).
19. A. A. Voronin and A. M. Zheltikov, Sci. Rep. **7**, 46111 (2017).
20. A. V. Mitrofanov, A. A. Voronin, D. A. Sidorov-Biryukov, M. V. Rozhko, E. A. Stepanov, A. B. Fedotov, V. Shumakova, S. Ališauskas, A. Pugžlys, A. Baltuška, and A. M. Zheltikov, Sci. Rep. **7**, 1 (2017).
21. Y. E. Geints and A. A. Zemlyanov, Appl. Opt. **56**, 1397 (2017).
22. Y. Silberberg, Opt. Lett. **15**, 1282 (1990).
23. G. Andriukaitis, T. Balčiūnas, S. Ališauskas, A. Pugžlys, A. Baltuška, T. Popmintchev, M.-C. Chen, M. M. Murnane, and H. C. Kapteyn, Opt. Lett. **36**, 2755 (2011).
24. A. V. Mitrofanov, A. A. Voronin, D. A. Sidorov-Biryukov, A. Pugžlys, E. A. Stepanov, G. Andriukaitis, T. Flöry, S. Ališauskas, A. B. Fedotov, A. Baltuška, and A. M. Zheltikov, Sci. Rep. **5**, 2 (2015).
25. P. Polynkin, Appl. Phys. Lett. **101**, 164102 (2012).
26. G. Agrawal, *Nonlinear Fiber Optics*, 5th ed. (Academic, 2013).
27. J. H. Marburger, Prog. Quantum Electron. **4**, 35 (1975).
28. A. Dubietis, G. Tamošauskas, G. Fibich, and B. Ilan, Opt. Lett. **29**, 1126 (2004).
29. A. V. Mitrofanov, A. A. Voronin, M. V. Rozhko, D. A. Sidorov-Biryukov, A. B. Fedotov, A. Pugžlys, V. Shumakova, S. Ališauskas, A. Baltuška, and A. M. Zheltikov, Optica **4**, 1405 (2017).
30. J. Santhanam and G. P. Agrawal, Opt. Commun. **222**, 413 (2003).